Available online at www.most.gov.bd

Volume 04, Issue (1), Page: 129-144, 2022

Ministry of Science and Technology
Government of The People's of Bangladesh
Bangladesh Secretariat, Dhaka.

Heat-Flux Effect on Fluid Flow and Convective Heat Transfer Through a Rotating Curved Micro-Channel

S. C. Adhikari, R. K. Chanda, R. Akter and R. N. Mondal*

Department of Mathematics, Jagannath University, Dhaka-1100, Bangladesh

Abstract

The present paper investigates heat-flux effect and the dissemination of energy in a rotating bent square micro-channel (MC) subject to a temperature gradient between the vertical sidewalls. The flow structure prevailing the problem is solved by applying a highly accurate spectral-based numerical scheme. The flow controlling parameters are the Dean number ($0<Dn\leq5000$) and the Taylor number ($-500 \leq Tr \leq 2000$) for curvature 0.01 and the Grashof number, $Gr=1000$. After applying the arc-length path continuation technique to obtain steady solution (SS) curves, two branches of SS consisting of 2- to 8-vortex solutions are prevailed for the non-rotating case while a single branch with a symmetric 2-vortex solution is for positive rotation of the channel. Unsteady flow (UF) properties are simulated by the time-average of the solutions, and the transitional behavior is well predicted by contemplating the power spectrum and phase spaces of the solutions. Results manifest that the UF experiences a consequence 'steady-state → multi-periodic → steady-state' for no rotation of the channel as *Dn* is increased. For the rotating case, on the other hand, the flow advances in the scenario 'steady-state → multi-periodic → steady-state' for negative rotation and only a steady-state solution for rotation in the positive direction. Streamlines and isotherms of SS and UF for various values of the flow-controlling parameters are obtained. Centrifugal force impacts the fluid mixer, which then assists to turn the flow into chaos and prompts to intensify the convective heat transfer (CHT).

Received: 15.01.2023
Revised: 27.03.2023
Accepted: 10.05.2023

DOI: https://doi.org/10.3329/jscitr.v4i1.67375

Keywords: Rotating micro-channel; Flow pattern; Unsteady solution; Phase space; Heat transfer.

Introduction

Flow characteristics especially rotating flows and heat transfer (HT) in a rotating system of different geometrical shapes has attracted a lot of attention from prodigious researchers due to plentiful applications in the engineering fields like heating and cooling system, rocket engine, electric generators, solar energy, and many more (Kockmann, 2005; Yi and Bau, 2003; Schonfeld and Hardt, 2004). The qualitative approach in micro-biochips, micro-fuel cells, micro-coolers, and micro-reactors has been increasing at a rapid cognition due to the quick advancements in nanoelectronics and bioengineering. Since the last couple of decades, research conducted in straight or curved MC has revealed that only a few scientific or numerical evaluations of the analysis of flow behavior in curved MC have been done. (Morini, 2004; Yang *et al.,* 2005; Wang and Liu, 2007). Microfluidic systems typically feature laminar flows, as opposed to the conventional flow processes found in macroscopic devices.

*Corresponding author's e-mail: rnmondal71@yahoo.com

Schönfeld and Hardt's (2004) work on curved MC showed that the induced secondary flows generate a mixing effect in micro-devices. The simulated results on helical flows by Jiang *et al.* (2004) verify the predicted mixing results by a series of experimental evaluations.

Rotating flow features are analyzed in three topics which are the steady solution (SS), unsteady solution (US), and CHT. Curved channel with rotation produces two forces; Centrifugal force and Coriolis force, and these forces directly impact the fluid flow and produce spiraling flow which is also called secondary flow (SF). The first evidence was provided by Dean (1927) where the existence of such kind of problem was analyzed and discussed in detail for motion in a curved tube with a circular cross-section. The main result of this analysis was to introduce the SF which was characterized by the Dean vortices, initiated by Dean in 1927. Since then, several enthusiastic researchers have given deep attention to investigating such types of fluids through different geometric shapes for rotation and non-rotation. Several landmark articles on curved duct flows are mentioned here, for example, Selmi *et al.* (1994), Alfredsson *et al.* (1989), Barua *et al.* (1954), Chengand Wu, (1970), Yamamoto *et al.* (1999), Yanase *et al.* (2002), Hasan *et al.* (2022a, 2022b).

Analyzing the bifurcation structure, which includes the SS and its linear stability, is one of the most important characteristics of fluid flow in a curved MC. Selmi *et al.* (1994) investigated the structure of bifurcation for an incompressible fluid in a rotating curved channel (CC). A 6-cell revolving flow phenomenon was discovered by Yamamoto *et al.* (1999) in their examination. Later, Mondal *et al.* (2007) and Adhikari *et al.* (2021) evaluated how the bifurcation diagram altered as the curvature of a non-rotating CC expanded or reduced and demonstrated the precise affinity to transient behavior and the bifurcation pattern among steady branches. Wang and Liu (2007) performed a computational analysis on a completely branching structure and stability in a bending MC with a square bend to inscribe the ramifications of curvature, initial circumstances, and disturbances. They showed thatregardless of duct curvature size, the spiraling flow is always produced in the channel. They observed multiple limiting points and asymmetric branching points in their ten branches of solutions. Other pertinent studies on fluid flow through different geometric circumstances include Chanda *et al.* (2020, 2021), Yamamoto *et al.* (2006), Mondal *et al.* (2014), and Hasan *et al.* (2019b).

Examining the nonlinear characteristics is important to figure out the unsteady behavior of the flow. Chandratilleke and Nursubyakto (2003) proposed a mathematical method for elucidating the flow characteristics using a variety of geometrical shapes with various aspect ratios. Later, Wang and Yang (2005) investigated the regular oscillations of an incompressible viscous fluid in a curved square channel (CSC) using both numerical and experimental methods, and a comparison of their findings revealed that they were completely consistent. Mondal *et al.* (2013, 2014) demonstrated the relationship between the UF and the bifurcation structure through linear stability. Through analyzing the oscillating behavior computationally by Mondal *et al.* (2017), regular and irregular oscillating flows were observed under conditions of symmetry and without symmetry, respectively. The majority of the important publications solely focused on weak rotational speed. Because of these questions to be answered, the current work focuses on how gyration and curvature affect the flow of unsteady fluid in a CRC.

Chandratilleke and Nursubyakto (2003) studied the role of Dean vortices in fostering HT and demonstrated that CC is more capable than that in a straight duct to gain a better knowledge of thermo-fluid dynamics and CHT through CC. The published simulation results of Yanase *et al.* (2002) and Mondal *et al.* (2014) show that SFs increase HT in the flow. The numerical method of flow characteristics and HT via a rotating CSC for different curvatures was recently carried out by Hasan *et al.* (2019a, 2019b). Recently, Roy *et al.* (2020) applied a method that used Hasan *et al.* (2019a) to prognosticate hydrodynamic unsteadiness and CHT in a rotating CRC of medium curvature. In this study, we present the numerical analysis of the puzzling flow behavior and energy distribution of fluid flow in a tightly coiled square-shaped micro-channel in a rotating system. Flow pattern as well as US of the flow features with CHT with strong rotational speed is investigated for both co-rotating and counter-rotating cases of the micro-channel.

Mathematical Model

The geometric scheme that is taken into consideration in this present study is shown in Figure 1. We have into account a fully formed 2D viscous incompressible, and thermally active fluid that passes through CSC. The fixed revolving speed of the system is Ω_T. The applied condition to the outside bend of geometry is at high temperature, on the other hand, the inner bend wall is kept at standard room temperature whereas both the upper surface and lower portion of the wall remain adiabatically isolated. It is presumed that a constant pressure gradient controls the fluid flow as shown in Fig. 1.

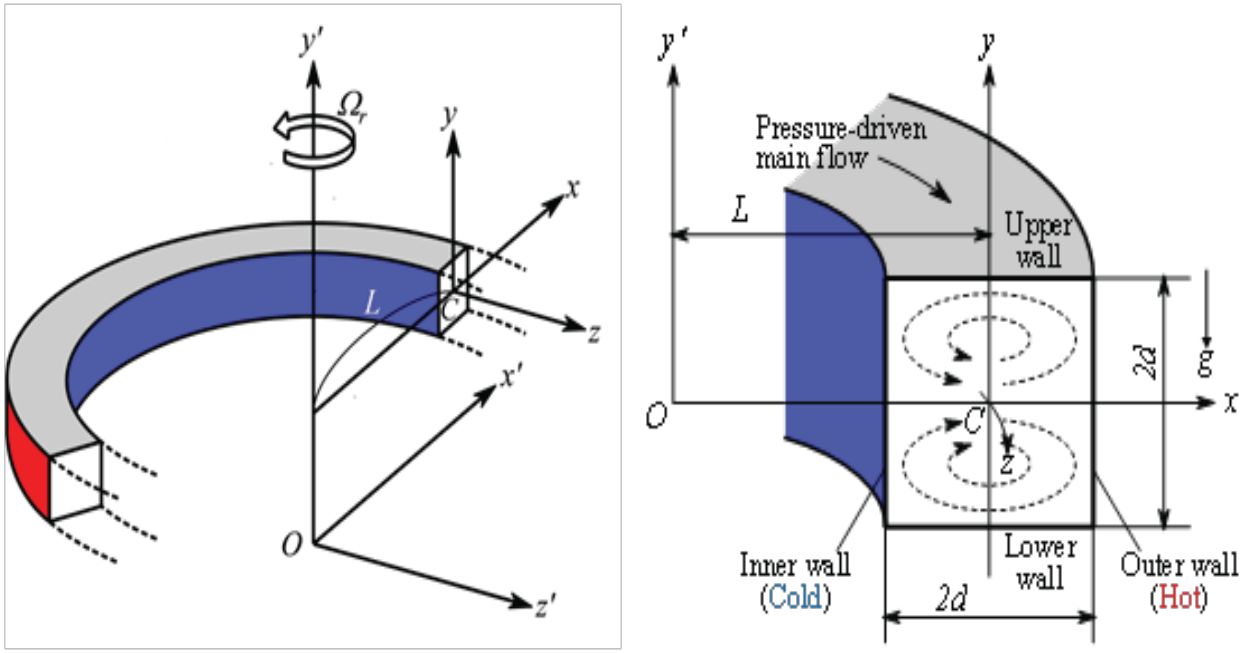

Fig. 1. Geometry of the problem.

The working equations such as the mass conservation, momentum equation, and energy equation which describe the physical situation of the flow through a revolving duct can be referred to as Chanda *et al.* (2020, 2021). Those equations are non-dimensionalized by using the following variables,

$$u=\frac{u'}{U_0},v=\frac{v'}{U_0},w=\frac{\sqrt{2\beta}}{\mathrm{U_o}}w',x=\left(\frac{x'}{d}-\frac{1}{\beta}\right),\bar{y}=\frac{y'}{d},z=\frac{z'}{d},P=\frac{P'}{\rho {U_0}^2},T=\frac{T'}{\Delta T'},t=\frac{U_0}{d}t',\beta=\frac{d}{L}$$

where, $U_0=\frac{\upsilon}{d}$ is the uniform velocity. Here, d and υ are the representative length and the kinematic viscosity respectively. Since our study is a two-dimensional case, so we assumed $\frac{\partial}{\partial z}=0$. Thus, the transform equations are as follows.

Mass conservation equation:

$$\frac{\partial u}{\partial x}+\frac{\partial v}{\partial y}+\ell\beta u=0 \tag{1}$$

Navier-Stokes equation:

$$\frac{\partial u}{\partial t}+\left(v\frac{\partial}{\partial y}+u\frac{\partial}{\partial x}\right)u-\frac{\in^2}{2}\ell w^2=-\frac{\partial P}{\partial x}+\frac{\in}{Dn}\left(\Delta_2 u-\ell^2\beta^2 u\right) \tag{2}$$

$$\frac{\partial v}{\partial t}+\left(v\frac{\partial}{\partial y}+u\frac{\partial}{\partial x}\right)v=-\frac{\partial P}{\partial y}+\frac{\in}{Dn}\Delta_2 v \tag{3}$$

$$\frac{\partial w}{\partial t}+\left(v\frac{\partial}{\partial y}+u\frac{\partial}{\partial x}\right)w+-\frac{\in^2}{2}luw=\ell G+\frac{\in}{Dn}\left(\Delta_2 w-\ell^2\beta^2 w\right) \tag{4}$$

where,

$$Dn=\sqrt{\frac{2d}{L}}\frac{U_0 d}{v},\ \in=\sqrt{\frac{2d}{L}}=\sqrt{2\beta}\left(0\le\beta\le1\right),\ G=-\frac{\partial P}{\partial z},\ \ell=\frac{1}{1+\beta x}$$

Introducing sectional stream function ψ as follows

$$u=\ell\frac{\partial\psi}{\partial\bar{y}},\ v=-\ell\frac{\partial\psi}{\partial x},\text{ where }\ \ell=\frac{1}{1+\beta x} \tag{5}$$

The processing equations for axial flow, secondary flow, and energy equations are as follows

$$\frac{1}{\ell}\frac{\partial w}{\partial t}+\frac{\partial(w,\psi)}{\partial(x,y)}-Dn+\ell\beta^2 w=\frac{1}{\ell}\Delta_2 w-\beta\ell\frac{\partial\psi}{\partial y}w+\beta\frac{\partial w}{\partial x} \tag{6}$$

$$\left(\Delta_2-\beta\ell\frac{\partial}{\partial x}\right)\frac{\partial\psi}{\partial t}=-\ell\frac{\partial(\Delta_2\psi,\psi)}{\partial(x,y)}+\beta\ell^2\left[\frac{\partial\psi}{\partial y}\left(2\Delta_2\psi-3\beta\ell\frac{\partial\psi}{\partial x}+\frac{\partial^2\psi}{\partial x^2}\right)-\frac{\partial\psi}{\partial x}\frac{\partial^2\psi}{\partial x\partial y}\right]$$
$$+\beta\ell^2\times\left[3\beta\frac{\partial^2\psi}{\partial x^2}-3\beta^2\ell\frac{\partial\psi}{\partial x}\right]-2\beta\ell\frac{\partial}{\partial x}\Delta_2\psi+w\frac{\partial w}{\partial y}+{\Delta_2}^2\psi-Gr\frac{1}{\ell}\frac{\partial T}{\partial x}-Tr\frac{\partial w}{\partial y}, \tag{7}$$

$$\frac{\partial T}{\partial t}+\ell\frac{\partial(T,\psi)}{\partial(x,y)}=\frac{1}{\Pr}\left(\Delta_2 T+\beta\ell\frac{\partial T}{\partial x}\right) \tag{8}$$

$$\text{where, }\Delta_2\equiv\frac{\partial^2}{\partial x^2}+\frac{\partial^2}{\partial y^2},\ \frac{\partial(T,\psi)}{\partial(x,y)}\equiv\frac{\partial T}{\partial x}\frac{\partial\psi}{\partial y}-\frac{\partial T}{\partial y}\frac{\partial\psi}{\partial x} \tag{9}$$

Where, *Dn, Gr*, *Tr*, and *Pr* are the important dimensionless variables that appear in equations (6) to (8), can be defined as; $Dn=\frac{Gd^3}{\mu\upsilon}\sqrt{\frac{2d}{L}}$; $Gr=\frac{\beta g\Delta Td^3}{\upsilon^2}$; $Tr=\frac{2\sqrt{2\beta}\Omega_T d^3}{\upsilon\delta}$; and $\Pr=\frac{\upsilon}{\kappa}$.

The no-slip boundary conditions are

$$w(\pm1,y)=w(x,\pm1)=\psi(\pm1,y)=\psi(x,\pm1)=\frac{\partial\psi}{\partial x}(\pm1,y)=\frac{\partial\psi}{\partial y}(x,\pm1)=0 \tag{10}$$

and the conditions for thermally heated walls are

$$\left.\begin{array}{l}T=1\text{ at }x=1,y=y\\T=-1,\text{ at }x=-1,y=y\\T(x,\pm1)=x\text{ at }x=x,y=\pm1\end{array}\right\} \tag{11}$$

The following symmetry criterion is fulfilled by a class of solutions with respect to $y = 0$.

$$\left.\begin{array}{c}y\Rightarrow-y\\w(x,y,t)\Rightarrow w(x,-y,t),\\\psi(x,y,t)\Rightarrow-\psi(x,-y,t),\\T(x,y,t)\Rightarrow-T(x,-y,t)\end{array}\right\} \tag{12}$$

Numerical calculation

The spectral approach is employed as a fundamental tool since the current study is entirely focused on numerical computation. The expansion of the polynomial functions $\phi_n(x)$ and $\psi_n(x)$, entails the variables in a group of functions comprised of Chebyshev polynomials is represented as

$$\left.\begin{aligned}\phi_n(x) &= (1-x^2)\,D_n(x),\\ \psi_n(x) &= (1-x^2)^2 D_n(x)\end{aligned}\right\} \tag{13}$$

where $D_n(x) = \cos(n\cos^{-1}(x))$ states the Chebyshev polynomial of n^{th} order. The flow representing parameters is expanded in terms of the expansion functions $\phi_n(x)$ and $\psi_n(x)$ as:

$$w(x,y,t) = \sum_{m=0}^{M}\sum_{n=0}^{N} w_{mn}(t)\,\varphi_m(x)\,\varphi_n(y) \tag{14}$$

$$\psi(x,y,t) = \sum_{m=0}^{M}\sum_{n=0}^{N} \psi_{mn}(t)\,\psi_m(x)\,\psi_n(y). \tag{15}$$

$$T(x,,y,t) = \sum_{m=0}^{M}\sum_{n=0}^{N} T_{mn}\,\varphi_m(x)\,\varphi_n(y) + x \tag{16}$$

where M is the number of truncations in the x-direction and N is the number of truncations in the y-direction, and w_{mn}, ψ_{mn} and T_{mn} are the coefficients of expansion. The collocation points (x_i, y_j) are taken to be

$$\left.\begin{aligned} x_i &= \cos\left[\pi\left(1-\frac{i}{M+2}\right)\right], \qquad i = 1,\ldots,M+1\\ y_j &= \cos\left[\pi\left(1-\frac{j}{N+2}\right)\right], \qquad j = 1,\ldots,N+1\end{aligned}\right\} \tag{17}$$

where $i = 1,\ldots,M+1$ and $j = 1,\ldots,N+1$.

Resistance coefficient

The represented quantities of the resistance coefficient (λ) and the mean axial velocity $\langle w^* \rangle$ are defined as

$$\lambda = \frac{4\sqrt{2\beta}Dn}{\langle w \rangle^2} \tag{18}$$

$$\langle w^* \rangle = \frac{v}{4\sqrt{2\beta}d} \int_{-1}^{1} dx \int_{-1}^{1} \overline{w}(x,y,t)dy \tag{19}$$

Nusselt number

The Nusselt number (*Nu*) is indexed as horizontal heat transfer by

$$Nu = -\frac{d^*}{\Delta T^*}\left\langle \left.\frac{\partial T^*}{\partial x^*}\right|_{x=0} \right\rangle. \tag{20}$$

The heat transmission rate from the inner walls to the fluid is not uniform due to temperature differences across the vertical sidewalls. Hence *Nu* varies on both heating and cooling sidewalls. We define the Nusselt number for the cooled (Nu_{τ_c}) and heated (Nu_{τ_h}) sidewalls for the unstable solutions as follows.

$$Nu_{\tau_c} = \frac{1}{2}\int_{-1}^{1} \left\langle \left\langle \left.\frac{\partial T}{\partial x}\right|_{x=-1} \right\rangle \right\rangle dy, \quad Nu_{\tau_h} = \frac{1}{2}\int_{-1}^{1} \left\langle \left\langle \left.\frac{\partial T}{\partial x}\right|_{x=1} \right\rangle \right\rangle dy \tag{21}$$

where $\langle\langle\ \rangle\rangle$ is the time-average over a period.

Validation of numerical result

This study's underlying algorithm's precision is guaranteed by grid accuracy. In light of this, it is crucial to evaluate the algorithm's effectiveness. We have shown the validation of numerical exactness by determining heat flux (*Q*) and axial flow (w). The following relationship is used to estimate the error percentage.

$$\varepsilon_p = \left|\frac{\text{current value-previous value}}{\text{current value}}\right| \times 100\%.$$

In this study, we consider five grid sizes, $16\times16, 18\times18, 20\times20, 22\times22, 24\times24$ i.e. $N = M$. The grid size of 20×20 was good enough to guarantee the accuracy of the solution as represented in Table 1.

Table 1. Validation of grid resolution.

Taylor Numbers	M	N	Q	% relative error of Q	$w(0,0)$	% relative error of w
	16	16	263.625863	---	350.003962	---
	18	18	263.624128	0.0006583	350.304573	0.0858141
$Tr = 250$	20	20	263.623865	0.0000997	350.523230	0.0623801
	22	22	263.623901	0.0000137	350.688033	0.0469941
	24	24	263.623940	0.0000148	350.815378	0.0362997
	16	16	433.202226	---	374.325551	---
	18	18	433.202329	0.0000238	374.606876	0.0750987
$Tr = -250$	20	20	433.203314	0.0002273	374.825926	0.0584404
	22	22	433.202391	0.0002131	374.989494	0.0436193
	24	24	433.202270	0.0000279	375.116285	0.0338004

Results and Discussion

Here, the completely formed 2D viscous incompressible fluid through a curved micro-channel (CMC) is computationally evaluated with rotating and non-rotating cases for curvature $\beta = 0.01$. For the non-rotating case, the Dean number, $0 < Dn \leq 5000$, is the flow-controlling parameter while for the rotating case, the Taylor number, $-500 \leq Tr \leq 2000$, controls the flow. Two cases arise in the present study:

Case I: Non-Rotating channel

Case II: Rotating channel

In the following, SS, time advancement, and HT are discussed, in detail, for the above-mentioned two cases.

Case I: Non-Rotating channel

Structure for Steady Solutions

As investigated by Mondal *et al.* (2007, 2013) for finding the steady solutions, our study prevailed in two branches of SS for $0 < Dn \leq 5000$, $Gr = 1000$, $\beta = 0.01$ (see Fig. 3). These two branches are called Branch 1 (solid red line) and Branch 2 (solid black line). According to Mondal *et al.* (2006) discussion, the path continuation approach is used to acquire the SS branches using a variety of initial hypotheses. The velocity of the non-isothermal flow and isotherm is shown in Fig. 4. It is clear that Branch 1 is made up of a sym-

metric 2- to 8-vortex solution, whereas Branch 2 is made up of a 4- to 8-vortex solution. Finally, the variation of velocity concerning grid points in the primary flow is depicted in Figure 5 which gives us the idea of CMC flows heating wall and cooling wall as shown in Figure 2.

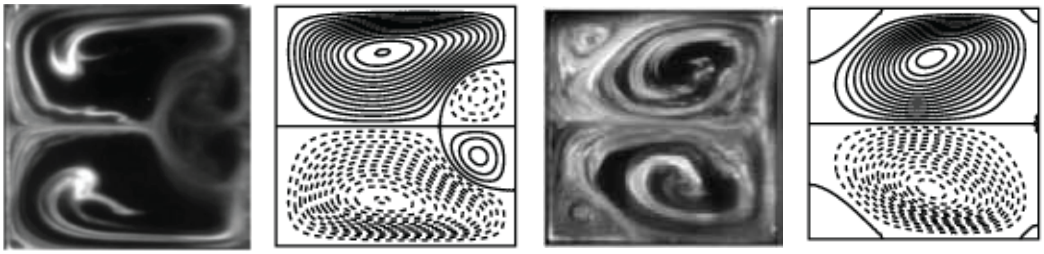

Fig. 2. Experimental vs. computational results for CSD flow (Left: Experimental and Right: computational result) (a) Positive rotation at *Tr* = 150, (b) Negative rotation at *Tr* = -150.

Unsteady solutions

By investigating the time-advancement solution for CMC with the heating wall and cooling wall for 0<Dn ≤3840, as visualized in Fig. 6, the unsteady flow is discovered to have a steady-state solution. Steady-state flow in this region always possesses a 2-vortex solution.The nature of the flow quickly changes to regular oscillation i.e., periodic as *Dn* increases. For 3845 ≤ *Dn* ≤ 4700, the unsteady flow (UF) remains in regular oscillation and the pattern of the secondary flow fluctuate in a certain range. The irregularities of the flow arise as seen in Fig. 6 for *Dn* = 5000. Contours of PF, SF, and thermoprofile are shown in Figure 7 for various *Dn* at the mentioned time. A 2-vortex asymmetric solution is remained up to the periodic stage and in the chaotic state, a new vortex is produced from the channel's outer wall. This new vortex is called *Dean-vortex* which is due to a high-pressure gradient. As seen from Figure 7, the velocity increases in the axial direction as *Dn* increases, and the contours of the isotherms distribute from the center of the outer lateral wall to the inner lateral wall because of the buoyancy force and curvature effect.

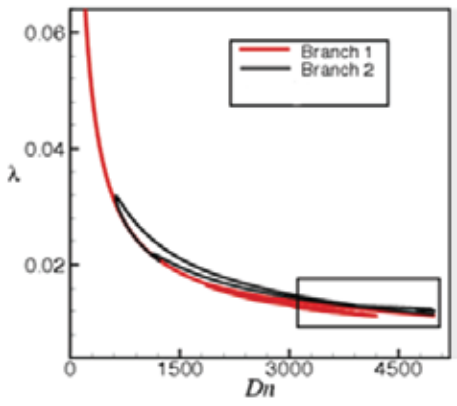

Fig. 3. Bifurcation structure of steady solutions.

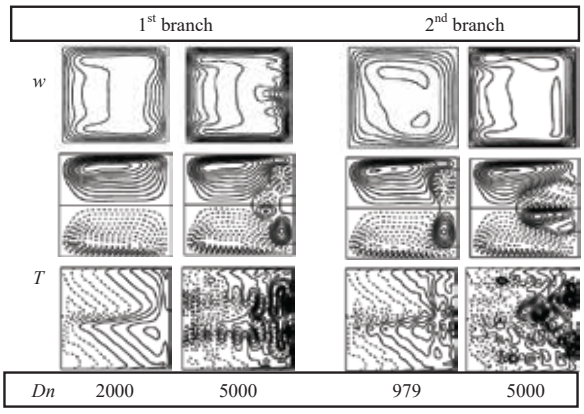

Fig. 4. Contours of primary flow (PF) (top), secondary flow (SF) (middle), and isotherm (bottom) for various *Dn*.

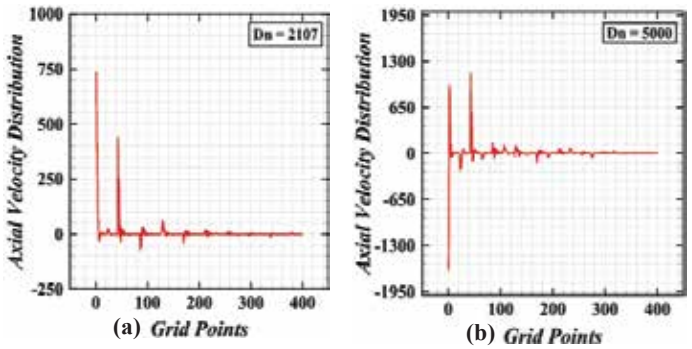

Fig. 5. Primary flow (axial flow) over grid points for non-rotating channel.

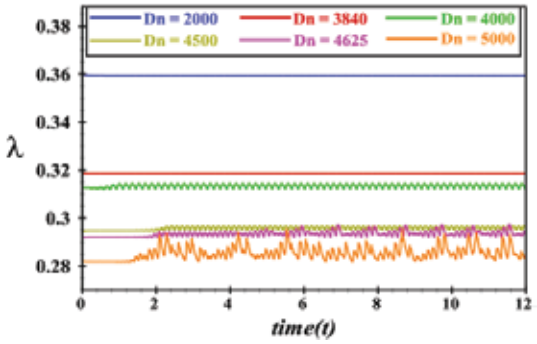

Fig. 6. Time-advancement of the flow for various *Dn's*.

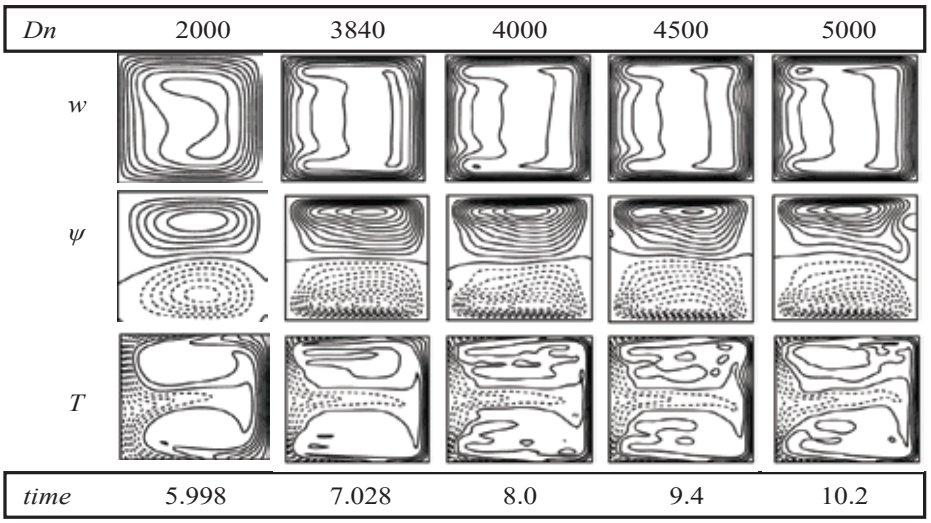

Fig. 7. Contours of PF (top), SF (middle), and isotherm (bottom).

Convective heat transfer (CHT)

To explore the CHT from the walls to fluid, we study temperature gradients (TG) which simply can explain the rate of heat at a particular location. The TGs are executed for some specific *Dn* values and presented for the cooled wall (CW) in Figure 8(a) and for the heated wall (HW) in Figure 8(b). It is noticed from Figure 8(a) that on the CW the temperature difference is $\left(\frac{\partial T}{\partial x}\right)$ dropped down in the middle region of the duct as *Dn* increases which are taken place due to the advection of outward SF as well as the influence of centrifugal force. On the contrary, outside the central region, $\left(\frac{\partial T}{\partial x}\right)$ is increased monotonically, which is resulted from the advection of inward SF and due to the fluid mixing. Besides, $\left(\frac{\partial T}{\partial x}\right)$ is prolonged at the central portion of the duct on the HW monotonically by the opposite SF in the inward direction.

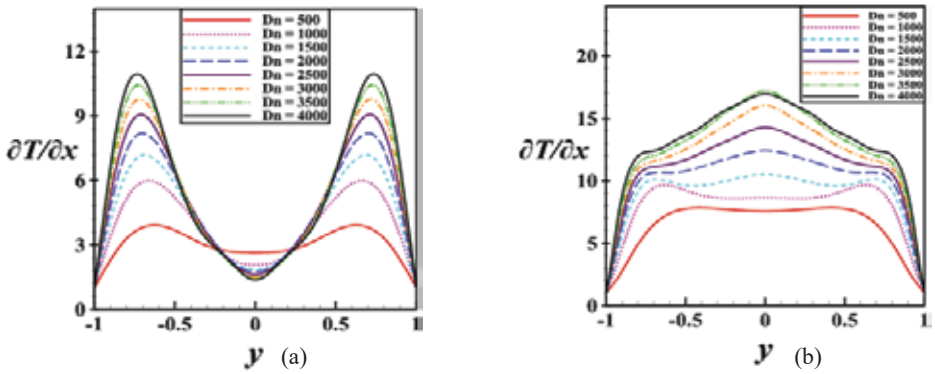

Fig. 8. TGs (a) at the cooling side; (b) at the heating side.

Case II: Rotating channel

Steady solutions for positive rotation

We have searched the SS branches with the help of the path continuation technique and arc-length method and obtained a single branch of SS which exists in the entire ranges for β = 0.01. Fig. 9 shows a unique SS branch, where we see that the branch is very simple. In Fig. 10, the contours of PF (up), SF (middle), and temperature profile (bottom) on the SS branch for β= 0.01at *Dn* = 2000, *Gr* = 1000, and for various values of *Tr* are demonstrated, where it is seen that the branch is composed of a symmetric 2-vortex solution. Due to the small curvature, Coriolis, and centrifugal forces, the primary velocity and isotherms only little altered as the rotation is increased. The velocity of the flow in the axial direction over various grid points is also shown in Figure 11 for *Tr* = 500 and *Tr* = 2000 which provides us the scenario of velocity increase in a rotating square channel flow for the heating wall and cooling wall.

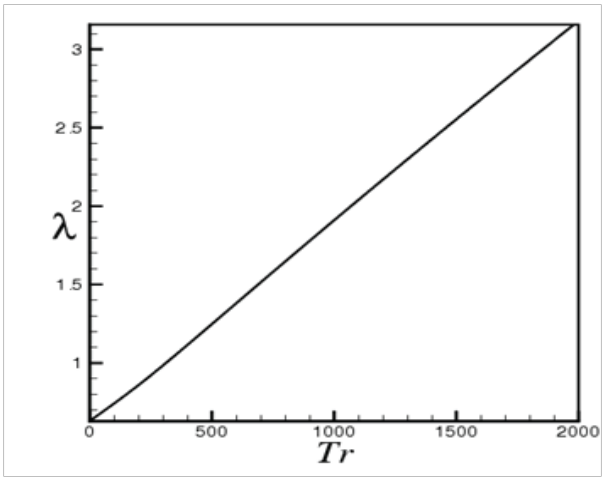

Fig. 9. Bifurcation structure of SS branch.

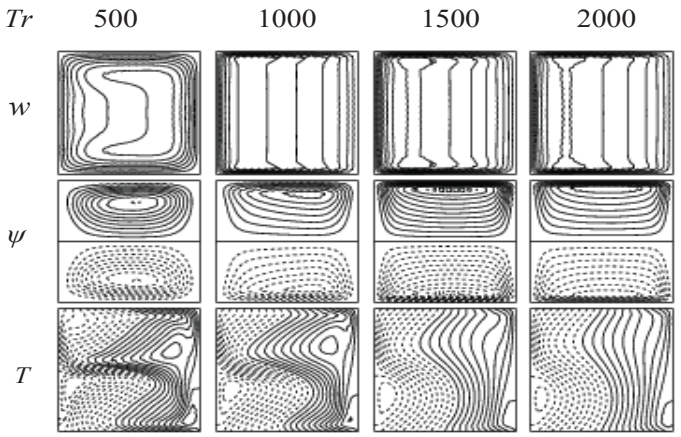

Fig. 10. Contours of PF (top), SF (middle), and temperature profile (bottom).

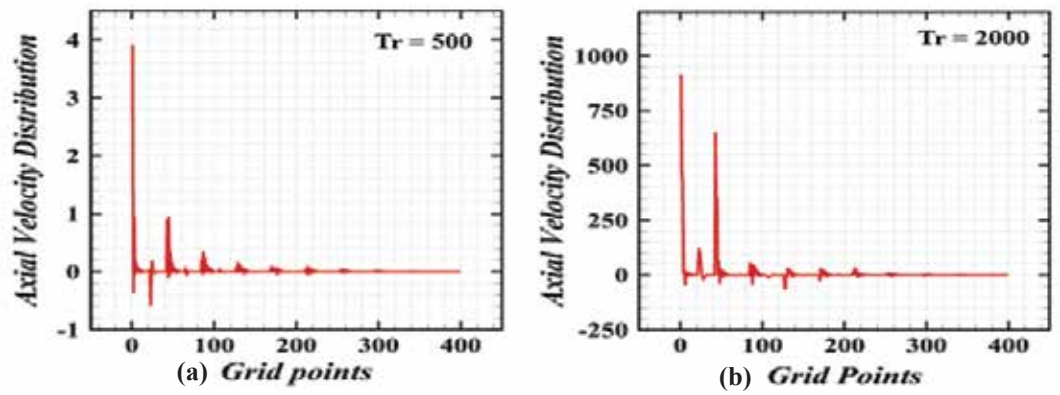

Fig. 11. Primary flow (axial flow) over grid points for rotating channel.

Unsteady solutions

We perform the time-dependent solution for β = 0.01at *Dn*= 2000 and *Gr* = 1000 for different values of *Tr*. The unsteady solution (US) of the entire domain of the investigated *Tr* (0<*Tr*≤2000) gives us the same result as the steady-state with a 2-vortex solution (see Fig. 12 and 13). There is no notable change occurring in the primary flow and temperature distribution and implicit with the secondary vortices.

Convective heat transfer (CHT)

To determine the CHT from the heatingwall to the fluid, the influence of positive rotation on the heat-generating mechanism is examined. We compute TG at the CW and HW for this reason. Fig. 14(a) illustrates how the difference in temperature on the HW grows in the central region owing to a slight vibration of the heating wall and varies in other places as a result of the fluid mixing. Figure 14(b) shows that $\left(\frac{\partial T}{\partial x}\right)$ on the CW diminishes in the middle area about *y* = 0 and $\left(\frac{\partial T}{\partial x}\right)$ gradually increasesthe whole part of the duct except the middle area. The propagation of the SF in an outward direction is what leads to these results around *y* = 0 because of the centrifugal force. These results demonstrate that when *Tr* rises, there is a substantial augmentation in heat transmission from the heating lateral wall to the fluid.

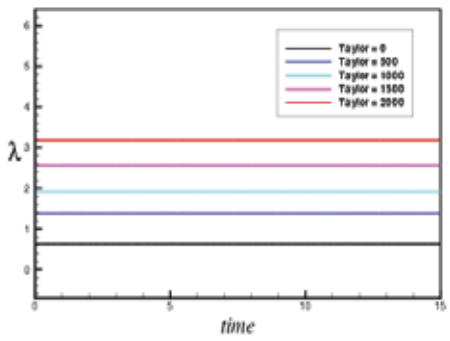

Fig. 12. Time advancement flow for various *Tr* at β = 0.01

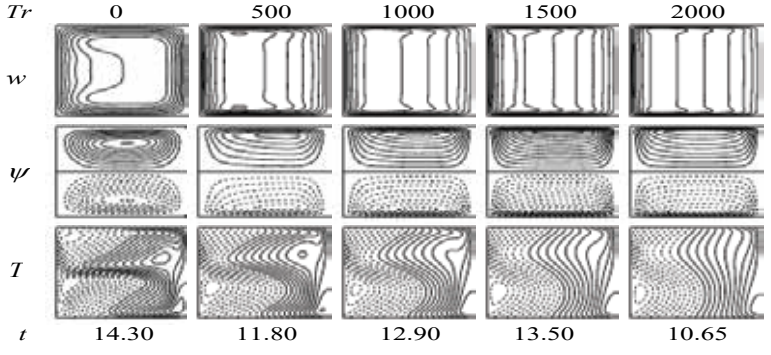

Fig. 13. Contours of PF (top), SF (middle) and temperature (bottom) profile for various *Tr*.

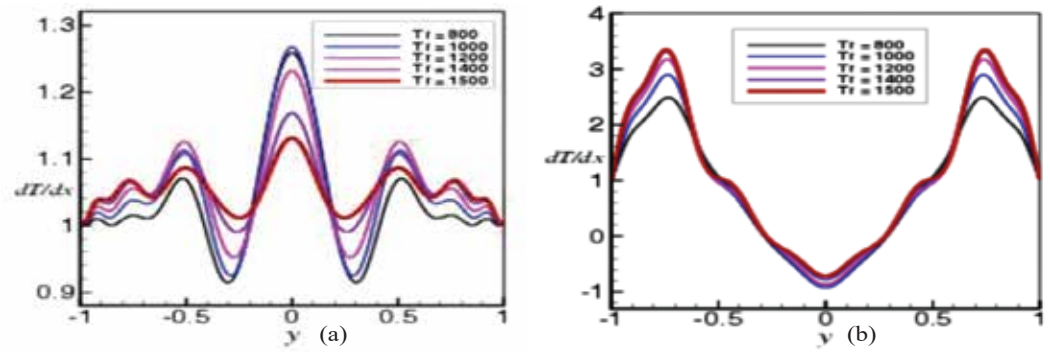

Fig. 14. TG for the rotating channel. (a) at the heatingwall; (b) at the cooling wall Negative Rotation: (β = 0.01, *Dn* = 2000, Gr = 1000, -500≤*Tr*<0).

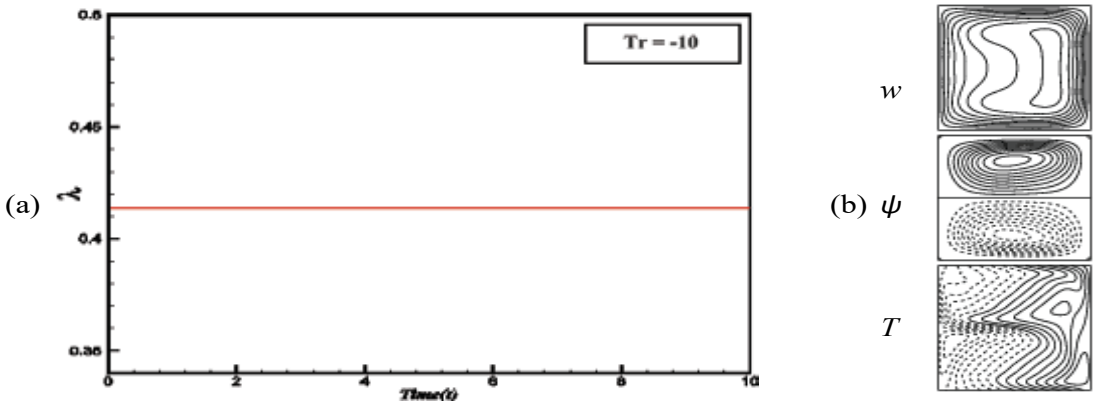

Fig. 15. (a) Transient solution for *Tr* = -10, (b) contours of PF (top) SF (middle), and temperature profile (bottom) for *Tr* = -10.

Here, we studied the transient flow behavior for negative rotation of the curved MC for -500≤*Tr*<0, *Dn* = 2000, *Gr*= 1000, and β = 0.01. Fig. 15(a) and 15(b) show that the UF is a steady-state with a 2-vortex solution for *Tr* = -10. When *Tr* = -250 then we see that the UF is multi-periodic with a 2- to 4-vortex solution (see Fig. 16 and 18). Fig. 17(a) and 17(b) demonstrate the phase-space diagram and spectrum density analysis for conformation of the multi-periodicity flow. Next, we investigate the UF for *Tr* = -500 where it can be

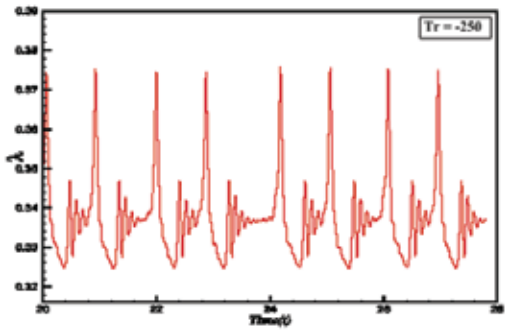

Fig. 16. Transient solution for *Tr* = -250 *and β* = 0.01 *at Dn* = 2000.

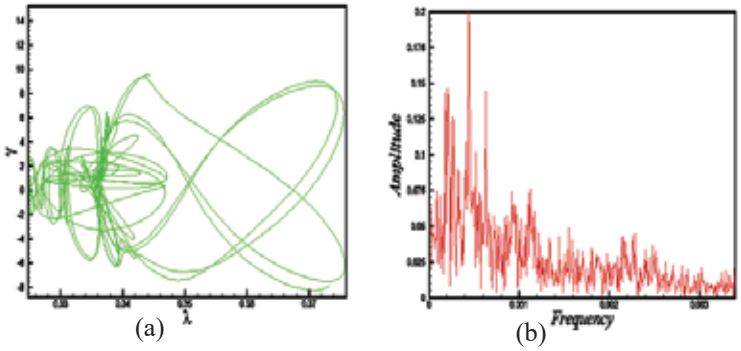

Fig. 17(a). Phase space (b) Power spectrum densityfor *Tr* = -250 and β = 0.01 at *Dn* = 2000.

visible that the UF returned to the previous state i.e., the steady-state but the remarkable scenario is that the UF is composed of a 4-cell solution (Fig. 19). The interaction among centrifugal, Coriolis, and buoyancy forces results in the formation of these vortices.

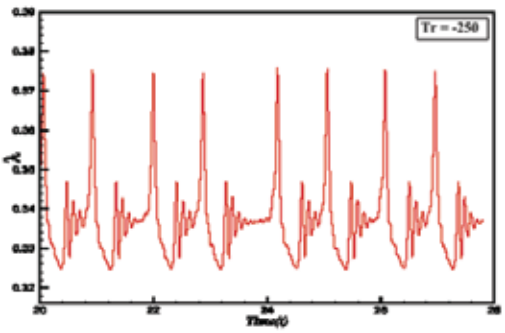

Fig. 16. Transient solution for *Tr* = -250 and β = 0.01 at *Dn* = 2000.

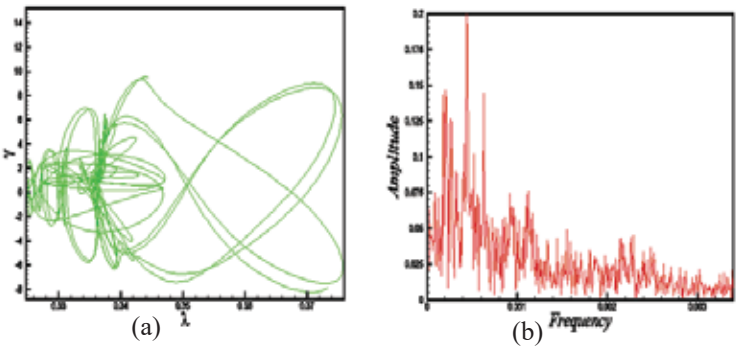

Fig. 17(a). Phase space(b) Power spectrum densityfor *Tr* = -250 and β = 0.01 at *Dn* = 2000.

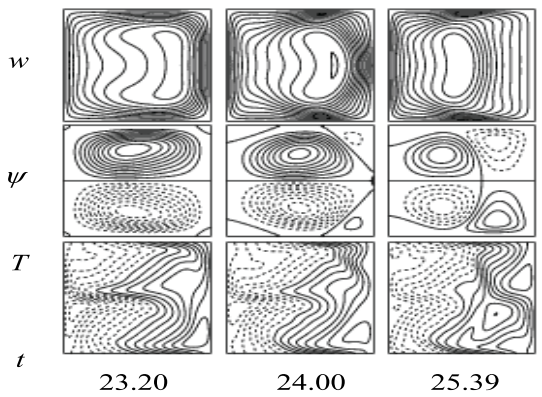

Fig. 18. Contours of PF (Up), SF (middle), and temperature profile (bottom) at for *Tr* = -250.

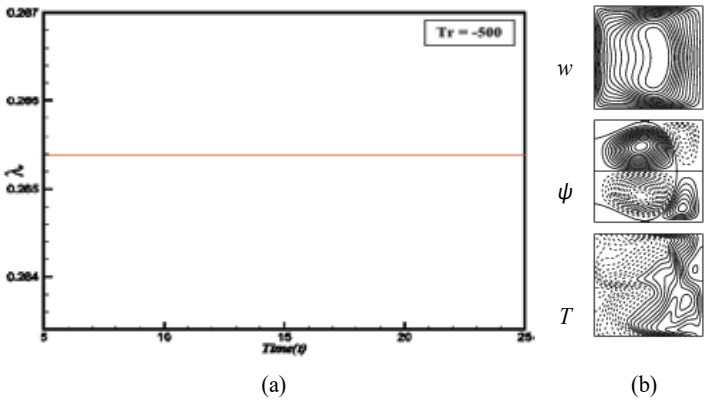

Fig. 19. (a) Transient solution for Tr = -500, (b) Contours of PF (Up), SF (middle), and temperature profile (bottom) for *Tr* = -500 at t = 20.

Vortex diagram in the plane

We demonstrate the structure fluctuation of secondary vortices for various parameters of *Tr* to observe the structure of SF in the light of vortices. Fig. 20 depicts how many vortices can the flow be formed for a specific value of curvature at a Taylor number and a two- to eight-vortex solution is discovered in the secondary flow pattern for distinct values of Tr. It has become possible to figure out maximum 8-vortex solutions for curvature β= 0.001, compared to 4- and 2-vortex solutions for β = 0.1 and β = 0.5 correspondingly. It is revealed that when *Tr* rises, the vortices' number falls. In this work, the steady-state solution has been discovered to have 2-vortex solutions, the periodic solution has 2- to 4-vortex solutions, and the chaotic solution has 2- to 6-vortex solutions. Due to the fact that chaotic solutions generate a large number of vortices in the surrounding concave wall, it is suggested that they be used instead of steady-state or periodic solutions to enhance heat transmission.

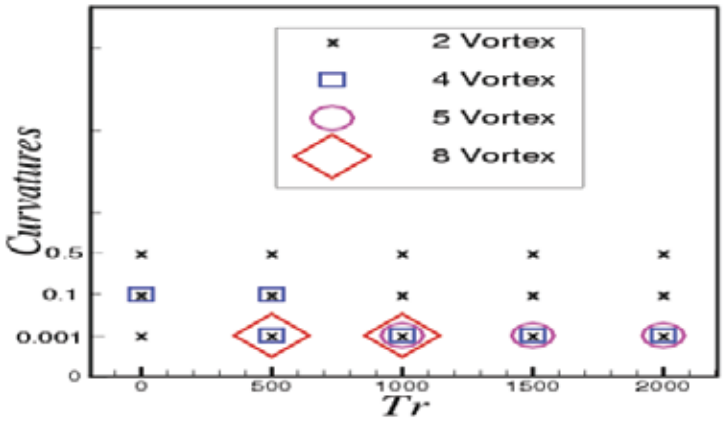

Fig. 20. Structure of secondary vortices for $0.001 \leq \beta \leq 0.5$ and $0 < Tr \leq 2000$.

Conclusions

In the present study, the heat-flux effect and the dissemination of energy through a bent MC are determined using a spectral-based computational scheme for rotating and non-rotating cases with a temperature gradient between the vertical lateral walls. From the present study, the following outcomes are listed:

- For non-rotating case, two asymmetric SS are revealed with 2- to 8-vortex solutions. The nonlinearity of the time-advancement flow demonstrates as 'steady-state periodic chaotic' which consists of a 2- to 4-vortex solution.
- For positive rotation, an asymmetric SS branchis found with a 2-vortex solution.The nonlinearity of the time-advancement flow is 'steady-state' only and consists of a two-vortex solution.
- By analyzing non-linear behavior for negative rotation, the unsteady flow goes through-'steady-state-multi-periodic steady-state' with a 2- to 4-vortex solution.
- CHT is increased significantly with the increase of *Dn* for non-rotating duct and imposing rotational speed i.e., raising *Tr* number. Higher *Tr* leads to the development of the extremely complicated secondary flow field.
- The research demonstrates that buoyancy force interacts with centrifugal and Coriolis forces hart impact the fluid mixing, which then assists to turn the flow into chaos and prompts the intensification of the convective heat transfer (CHT).

Acknowledgment

Rabindra Nath Mondal, the corresponding author, would like to gratefully acknowledge the financial support from Bangladesh Ministry of Science and Technology (MOST) to conduct this research work under special allocation in 2020-2021 (No. 39.00.0000.009.14.011.20- Phy's-572).

References

Adhikari SC, Chanda RK, Bhowmick S, Mondal RN and Saha SC 2021. Pressure-Induced Instability Characteristics of a Transient Flow and Energy Distribution through a Loosely Bent Square Duct. *Energy Engineering* **119**(1): 429-451.

Alfredsson PA and Persson H 1989. Instabilities in channel flow with system rotation. *J. Fluid Mech.* **202:** 543–557.

Barua SN 1954. On secondary flow in stationary curved pipes. Proc. R. Soc. Lond. A. **227:** 133–139.

Chandratilleke TT and Nursubyakto 2003. Numerical prediction of secondary flow and convective heat transfer in externally heated curved rectangular ducts, *Int. J. Thermal Sci,* **42:** 187-198.

Chanda RK, Hasan MS, Alam M and Mondal RN 2021. Taylor-heat flux effect on fluid flow and heat transfer in a curved

rectangular duct with rotation. *International Journal of Applied and Computational Mathematics* **7**(4): 1-31.

Chanda RK, Hasan MS, Alam MM and Mondal RN 2020. Hydrothermal behavior of transient fluid flow and heat transfer through a rotating curved rectangular duct with natural and forced convection. *Mathematical Modelling of Engineering Problems* **7**(4): 501-514.

Cheng H and Wu TT 1970. Limit of cross sections at infinite energy. *Physical Review Letters* **24**(25): 1456.

Dean WR 1927. Note on the motion of fluid in a curved pipe. *Philos Mag.* **4:** 208-223.

Gottlieb D and Orszag SA 1997. Numerical analysis of Spectral Method, *Society for Industrial and Applied Mathematics, Philadelphia. U.S.A.*

Hasan MS, Mondal RN and Lorenzini G 2019a. Numerical Prediction of Non-isothermal Flow with Convective Heat Transfer through a Rotating Curved Square Channel with Bottom Wall Heating and Cooling from the Ceiling, *Int. J. Heat and Technology* **37**(3): 710-720.

Hasan MS, Mondal RN and Lorenzini G 2019b. Centrifugal Instability with Convective Heat Transfer through a Tightly Coiled Square Duct, *Mathematical Modelling of Engineering Problems* **6**(3): 397-408.

Hasan MS, Chanda RK, Mondal RN and Lorenzini G 2022a. Effects of rotation on unsteady fluid flow and forced convection in the rotating curved square duct with a small curvature. Facta Universitatis, Series: *Mechanical Engineering* **20**(2): 255-278.

Hasan MS, Mondal RN, Islam MZ and Lorenzini G 2022b. Physics of coriolis-energy force in bifurcation and flow transition through a tightly twisted square tube. *Chinese Journal of Physics* **77:** 1305-1330.

Jiang F, Drese KS, Hardt S, Küpper M and Schönfeld F 2004. Helical flows and chaotic mixing in curved micro channels. *AIChE Journal, Vol.* **50**(9): 2297-2305.

Kockmann N, Engler M, Haller D and Woias P 2005. Fluid dynamics and transfer processed in bended microchannels, *Heat Transfer Engineering* **26:** 71-78.

Mondal RN, Kaga Y, Hyakutake T and Yanase S 2006. Effects of curvature and convective heat transfer in curved square duct flows. Trans. ASME, *Journal of Fluids Engineering,* **128**(9): 1013-1022.

Mondal RN, Kaga Y, Hyakutake T and Yanase S 2007. Bifurcation diagram for two-dimensional steady flow and unsteady solutions in a curved square duct, *Fluid Dynamics Research* **39:** 413-446.

Mondal RN, Islam MS, Uddin K and Hossain MA 2013. Effects of aspect ratio on unsteady solutions through curved duct flow, *Applied Mathematics and Mechanics,* **34**(9): 1107–1122.

Mondal RN, Ray SC and Islam S 2014. Solution structure, stability and pattern variation of secondary flows through a rotating curved duct with rectangular cross section, *International Journal of Energy & Technology* **6**(5): 1-12.

Mondal RN, Ray SC and Yanase S 2014. Combined Effects of Centrifugal and Coriolis Instability of the Flow through a Rotating Curved Duct with Rectangular Cross Section. *Open Journal of Fluid Dynamics* **4:** 1-14.

Mondal RN, Watanabe T, Hossain MA, Yanase S 2017. Vortex-Structure and Unsteady Solutions with Convective Heat Transfer through a Curved Duct, *J. of Thermophysics and Heat Transfer* **31**(1): 243-254.

Morini GL 2004. Single-phase convective heat transfer in microchannels: a review of experimental results, *Int. J. Thermal Sciences* **43:** 631-651.

Roy SC, Hasan MS and Mondal RN 2020. On the Onset of Hydrodynamic Instability with Convective Heat Transfer through a Rotating Curved Rectangular Duct, *Mathematical Modelling of Engineering Problems* **7**(1): 31-44.

Schonfeld F and Hardt S 2004. Simulation of helical flows in curved microchannels, *AIChE Journal* **50:** 771-778.

Selmi M, Nandakumar K and Finlay WH 1994. A bifurcation study of viscous flow through a rotating curved duct, *J. Fluid Mechanics* **262:** 353-375.

Wang L and Yang T 2005. Periodic oscillation in curved duct flows. *Physica D,* **200:** 296-302.

Wang LQ and Liu F 2007. Forced convection in slightly curved microchannels, *Int. J. Heat and Mass Transfer,* **50**(5-6): 881–896.

Yamamoto K, Yanase S and Alam MM 1999. Flow through a rotating curved duct with square cross-section. *Journal of the physical society of Japan,* **68**(4): 1173-1184.

Yamamoto K, Wu X, Nozaki K and Hayamizu Y 2006. Visualization of Taylor-Dean Flow in a Curved Duct of Square Cross-Section. *Fluid Dynamics Research* **38:** 1-18.

Yanase S, Kaga Y and Daikai R 2002. Laminar flow through a curved rectangular duct over a wide range of the aspect ratio, *Fluid Dynamics Research* **31:** 151-183.

Yang WH, Zhang JZ and Cheng H 2005. The study of flow characteristics of curved microchannel, *Applied Thermal Engineering* **25**(13): 1894–1907.

Yi M and Bau HH 2003. The kinematics of bend-induced mixing in micro-conduits. *Int. J. Heat and Fluid Flow,* **24** 645-656.